Impact of titania phase structure and surface reactivity on the photocatalytic degradation of various dyes and textile wastewater

Hüsnü Arda Yurtsever*,[1], Onur İloğlu[1] & Muhsin Çiftçioğlu[2]

[1]Department of Materials Science and Engineering, Adana Alparslan Türkeş Science and Technology University, Adana, Turkey
[2]Department of Chemical Engineering, Izmir Institute of Technology, Izmir, Turkey
E-mail: husnuarda@gmail.com, hayurtsever@atu.edu.tr, muhsinciftcioglu@iyte.edu.tr

Titania (TiO_2) powders have been prepared by precipitation method in different precipitation media which contain sulfate, nitrate or organic species. Photocatalytic degradation of different dyes and a real textile wastewater have been conducted with these powders along with commercial powder Degussa P25 for comparison. Ethyl alcohol (organic medium), sulfuric acid (sulfate medium) and nitric acid (nitrate medium) have been used to dissolve titanium precursor for the precipitation of TiO_2 in ammonia solution. UV-Vis DRS and XPS results indicate that S doping in sulfate medium precipitated powder and N doping in nitrate medium precipitated powder has been occurred and the presence of S or N containing impurities on the grain boundaries have been improved light absorption of TiO_2 significantly. However, these powders have exhibited low surface reactivities. The highest surface reactivity has been obtained with the powder precipitated in organic medium which also has the highest crystallite sizes (76 nm rutile and 34 nm anatase crystallites) with relatively low rutile weight percentage (10.0%). The surface-normalized rate constants of this powder are 0.02038 $min^{-1}.m^{-2}$ in real textile wastewater degradation and 0.0161 $min^{-1}.m^{-2}$ in methyl orange degradation, which are 0.01563 and 0.0091 $min^{-1}.m^{-2}$, respectively, for Degussa P25. Results have shown that this powder show 30-70% higher surface reactivities compared to Degussa P25. The main structural difference of organic medium precipitated powder and Degussa P25 has been found to be the anatase-rutile weight ratio and crystallite size of rutile phase whereas band gap energy of Degussa P25 is lower and other properties are not significantly different.

Keywords: Crystal structure, Photocatalysis, Surface properties, Textile wastewater, Titania

Inorganic oxide materials (TiO_2, ZnO, CeO_2 etc.) are commonly preferred in photocatalysis due to their high corrosion resistance, thermal and photochemical stability and economic feasibility with high and efficient light absorption[1]. Titania (TiO_2) is a widely used material in environmental related photocatalytic research and applications. The major drawback in the use of TiO_2 in photocatalysis is its low solar light absorption capacity which is only in the UV light region. Nanostructure and electronic properties of TiO_2 (e.g. light absorption) can be altered by; doping with various cations/anions[2], combining with low bandgap materials[3], surface modification[4] or using different synthesis routes to modify the crystalline structure[5,6]. The reduction and modification of the band gap energy of TiO_2 by doping for more efficient absorption in the visible region and enhancement of the activity in dye degradation[7] and solar hydrogen generation is the main concern of intense global research effort in the last 10-15 years. Dopants intensely investigated in environmental related research comprise heavily nonmetals like C, N or S[8-12] and transition metals like Cu, Ag, Fe, Co[2,13,14] and rare earth metals like La, Nd[15,16]. Doping TiO_2 with nonmetals (C, S or N) can cause red-shift in the absorption threshold of TiO_2 which is believed to be due to the substitutional exchange with O atoms and mixing nonmetal 2p with oxygen 2p forming donor states above the valence band of TiO_2[17,18].

Commercial and mostly pure TiO_2 powders were used in a few studies towards the photocatalytic degradation of real textile wastewaters (RTW)[19-24]. Simulated textile wastewaters were also prepared by using commercially available dyes such as Basic Blue 41(Ref.25), Orange II, Orange G, Congo Red[26], AB 25(Ref.27), Reactive Orange 16(Ref. 28) and photocatalytic degradation of these dyes were performed by using mostly TiO_2 powders.

Industrial applications of photocatalytic water treatment processes are feasible when the photocatalyst powders are used on supports as thin/thick films due to no need of an extra purification step such as

photocatalyst powder removal. In this context, it is important to report the surface-normalized photocatalytic activity as it is implied by Wachs *et al*. θ. According to IUPAC recommendations, in heterogeneous photocatalysis, surface area normalized turnover frequency should be reported when the number of active sites is not known[30]. Hence, photocatalytic activity results can be interpreted more accurate according to surface related properties such as crystalline phase properties, band gap energy, surface chemistry and etc. The development of a better understanding between powder properties and photocatalytic decomposition kinetics would contribute significantly to a wider use of photocatalysis in environmental applications from an industrial application point of view.

In this study TiO$_2$ powders were prepared by using precipitation method. The effects of the chemistry of precipitation medium (containing organic, nitrate or sulfate based species) on the properties and surface reactivity of the powders were reported. Their performances in the treatment of synthetic dyes and RTW were investigated. The surface reactivities of the prepared powders were correlated with the surface physicochemical properties and some powder property optimizations were also suggested.

Experimental Section

Powder preparation

TiO$_2$ powders, which were also used in our previous study[31], were prepared by using a simple chemical precipitation method. Two precipitates (inorganic based) were prepared from titanium precursor titanium tetra-isopropoxide (TTIP) which was dissolved in two different inorganic solutions and one precipitate was prepared from organic solution. Commercial powder Degussa P25 was used without any modification.

Briefly, for the preparation of inorganic based precipitates, TTIP was first hydrolyzed by water, then dissolved in acidic solutions and finally precipitated in ammonia solution. Nitric acid and sulfuric acid were used to prepare the acidic solutions. Third precipitate (organic based) was prepared by the dropwise addition of ethanolic TTIP solution to ethanolic ammonia solution. All the prepared precipitates were dried at 70°C overnight and then subjected to heat treatment at 600°C for 3 h. Powders obtained after heat treatment were coded as OMP, NMP and SMP for organic medium precipitated (TTIP dissolved in ethanol), nitrate medium

precipitated (precipitate dissolved in nitric acid solution) and sulfate medium precipitated (precipitate dissolved in sulfuric acid solution), respectively. The codes of the powders were AP, NP and SP, respectively, in our previous study[31].

Powder characterization

Phase characterization including determination of crystallite size, rutile weight percentage, lattice constants and lattice strain by X-ray diffraction, elemental analysis by X-ray photoelectron spectroscopy, specific surface area determination by nitrogen adsorption-desorption analysis and band gap energy determination by UV-Vis diffuse reflectance spectroscopy were conducted by using the procedures described in our previous study[31]. Dynamic light scattering (DLS) analyses were conducted with Malvern Zetasizer 3000HSA for the determination of the particle size distributions of the powders. Room temperature photoluminescence (PL) emission spectra obtained upon 285 nm excitation wavelength were recorded on Varian Cary Eclipse fluorescence spectrometer.

Crystallite size was calculated by using Scherrer's equation (Eq. 1):

$$d = \frac{k.\lambda}{\beta.cos\theta} \qquad \qquad .. (1)$$

where, d is the crystallite size, k is a constant, λ is the x-ray wavelength, β is the full width at half maximum of the selected peak (main peaks of anatase and rutile phases) and θ is the Bragg's diffraction angle. Rutile weight percentage was calculated according to Eq. (2):

$$x_R = 1 - \left(1 + 1.26\frac{I_R}{I_A}\right)^{-1} \qquad \qquad …(2)$$

where, X$_R$ is the rutile weight percentage, I$_R$ and I$_A$ are the intensities of main diffraction peaks of rutile and anatase phases, respectively. Lattice constants were calculated by Eq. (3)

$$\frac{1}{d_{hkl}^2} = \frac{h^2+k^2}{a^2} + \frac{l^2}{c^2} \qquad \qquad …(3)$$

where, hkl are the Miller indices and d$_{hkl}$ is the interplanar spacing. Lattice strain was calculated by slope of the Williamson-Hall plot drawn by using Eq. (4) in which at least four diffraction angles were used

$$\frac{\beta cos\theta}{\lambda} = \frac{1}{\sigma} + \frac{\eta.sin\theta}{\lambda} \qquad \qquad …(4)$$

where σ is particle size and η is strain. Band gap energy was calculated by using Kubelka-Munk equation (Eq. 5):

$$F(R) = \frac{(1-R)^n}{2R} \qquad \qquad \dots(5)$$

where, F(R) is the Kubelka-Munk function, R is reflectance and n = 0.5 for indirect transition. In elemental analysis peak fit was conducted by using XPS Peak Fit 4.1 software program to determine the appropriate peak positions and C1s peak at 284.8 eV was used as the reference peak.

Photocatalytic degradation of synthetic dyes and real textile wastewater

The activities of the powders in the photocatalytic degradation of synthetic dyes (methylene blue, methyl orange and rhodamin B) were determined by using laboratory-made setup which consists of an inner irradiated PYREX photoreactor equipped with a 9W UV-A lamp (main emission peak at 365 nm). The activities in the photocatalytic degradation of the real textile wastewater were determined using the setup consisting of an externally irradiated pyrex photoreactor (133 ml), osram ultravitalux (300 W) lamp as the UV-Vis source with a solar-like irradiation spectrum according to the manufacturer and a cooling fan. This setup was used in order to simulate the solar like conditions for the photocatalytic degradation of real textile wastewater. The reaction temperature was kept between 40-45°C by the cooling fan. In each case, photocatalyst particles (0.1 g) were suspended in the dye solutions 230 mL, 10 ppm mL synthetic dyes and in 100 mL real textile wastewater which was obtained from a local plant. Powder suspensions were ultrasonicated for 1-2 min to increase the dispersion of the photocatalyst powders in the reaction medium and the illumination was started. The reaction mixtures were stirred during the photocatalytic experiments by a magnetic bar. Samples of 1 mL volume were withdrawn from the reaction mixture, centrifuged and analyzed with UV-Vis spectrophotometer. Pt-Co colour, *p*H and conductivity measurements of the textile wastewater samples were conducted by using Hach-Lange DR 3900 spectrophotometer and Hach-Lange HQ40d portable multimeter, respectively. The photocatalytic degradation experiments were also performed with the commercial powder Degussa P25.

UV-Vis spectra of the samples were recorded in the 300-800 nm wavelength range. The maximum absorption wavelengths of the dyes and wastewater were used for the determination of the dye concentrations used in the calculation of surface-normalized degradation (C_S)[32], surface-normalized 1st orderreaction

rate constants and degradation efficiencies (%) as shown in equations 6, 7 and 8, respectively.

$$C_S \left(\frac{mMdegradeddyeorppmRTW}{m^2} \right) = \frac{C_0 - C_t}{S_{BET}} \dots(6)$$

$$\text{Surface-normalized 1}^{st}\text{ orderreactionrateconstant} = \text{slope of } \frac{Ln\left(\frac{C_0}{C}\right)}{S} \qquad \dots(7)$$

$$\text{Efficiency (\%)} = \left(1 - \frac{C_t}{C_0}\right) x100 \qquad \dots(8)$$

Results and Discussion

Characterization

Phase characterization (XRD), optical characterization (UV-Vis DRS), surface area (Nitrogen adsorption-desorption) analysis and elemental analysis (XPS) results from our previous study[31] along with results from newly conducted photoluminescence (PL) analysis and particle size distribution analysis (DLS) were presented for the better understanding of the relation between the structural properties and surface reactivities in the photocatalytic degradation of dyes.

XRD patterns of the powders prepared with different precipitation media and commercial Degussa P25 powder are given in Fig. 1(a). Anatase phase (JCPDS Card #84-1286) was found to be the dominant phase among the powders whereas it is the only phase detected in SMP powder. A mixture of anatase-rutile (JCPDS Card #87-0920) phases were identified in OMP and NMP powders. Anatase crystallite size, bulk particle size, rutile wt.(%) and lattice constants of the powders are summarized in Table 1. The crystallite sizes vary from 34 nm to 18 nm in the order of OMP>NMP>SMP. Rutile wt. (%) was the highest in NMP powder. The lowest lattice constant c value for the anatase phase was calculated as 9.312 Å for SMP powder. Lattice constants depend heavily on the crystallite size, hence the lowest crystallite size of SMP may have led to the lowest lattice constant. SMP powder also showed the highest lattice strain which is probably due to having lower crystallite size. Lattice strain is known to originate from the interplay of the surface charge and grain boundary effects in nanostructures. The variation of strain among the powders was determined to be significant which is most probably due to the significant differences in the crystallite sizes. The highest and lowest tensile strains were calculated for SMP and NMP powders, respectively. Anatase to rutile phase transformation in OMP and NMP powders may have occurred at a lower temperature which may be an indication of structural stabilization
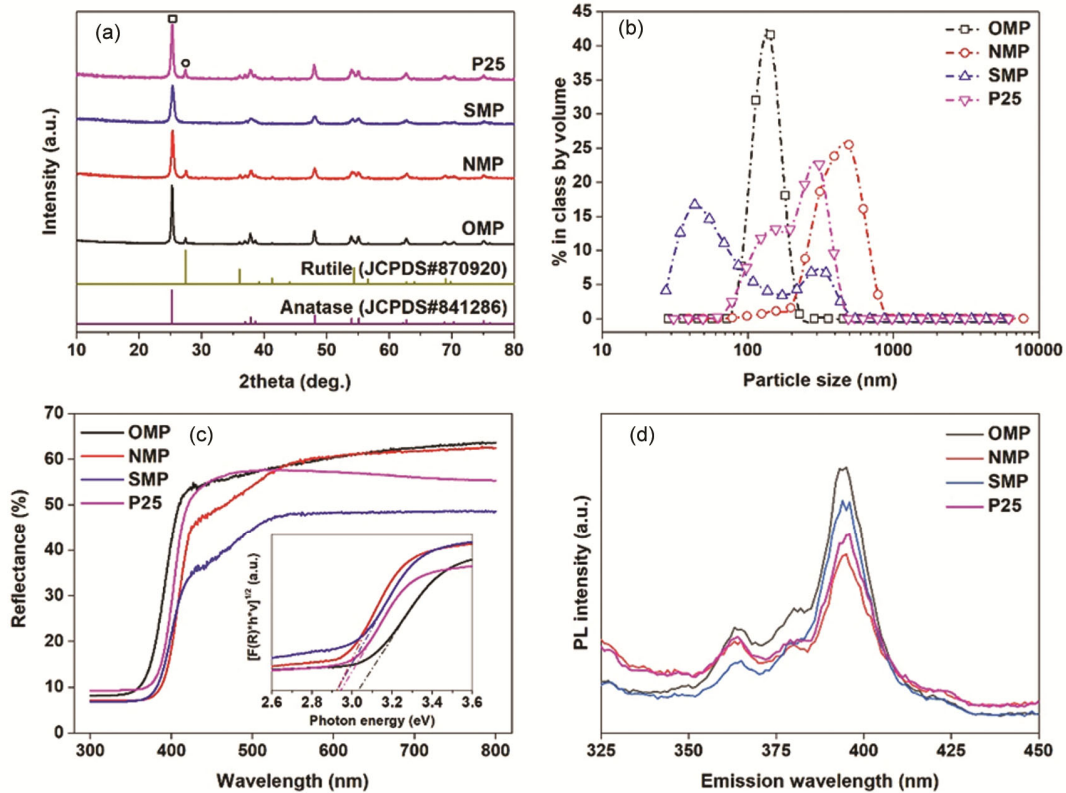
Fig. 1 — (a) XRD patterns (□: Anatase, o: Rutile), (b) Particle size distribution curves, (c) UV-Vis DRS spectra, plots of [F(R)*h*v]$^{0.5}$ versus photon energy (inset) and (d) Room temperature PL spectra of the powders. XRD and UV-Vis DRS data were "Reprinted from International Journal of Hydrogen Energy, Vol 43, Hüsnü Arda Yurtsever and Muhsin Çiftçioğlu, The effect of powder preparation method on the artificial photosynthesis activities of neodymium doped titania powders, 20162-20175, Copyright (2018), with permission from Elsevier[31].

at lower temperatures with a less defective structure compared to SMP powder. Fewer defects may lead to lower stress in the nanostructure.

Particle size distribution curves of the powders are given in Fig. 1(b). The average bulk particle size and anatase crystallite size were determined to be the lowest in SMP powder. The average bulk particle sizes were variable which may be due to variable crystallite sizes and phase composition in the powders. Hydrodynamic particle diameter (bulk particle size) measured by DLS technique increases with increasing heat treatment temperature as discussed by Shah *et al.*[33]. Hence, it may be stated that increase in the heat treatment temperature causes an increase in the primary particle sizes (anatase or rutile crystallites) which eventually causes an increase in the hydrodynamic particle diameter. In our study, all the powders were subjected to the same grinding process and the powder with lower primary particle size (crystallite size), SMP powder, possessed the lowest hydrodynamic particle diameter. The presence

of relatively higher number of rutile crystallites may also have increased the average bulk particle size as observed in NMP powder and P25 which have almost the same crystallite size and rutile weight percentages. OMP powder with the highest anatase and rutile crystallite size and moderate rutile weight percentage exhibited moderate bulk particle size with a narrow size distribution. It is expected that a photocatalyst particle with lower hydrodynamic diameter would show a better photocatalytic performance since low hydrodynamic diameter may lead to high surface area and photocatalytic rate significantly depends on the magnitude of the area of reaction interface. Thus, using surface-normalized reaction rate would be helpful to eliminate the surface area related properties when reporting the sole effect of phase structure on the surface reactivity of TiO$_2$.

UV-Vis DRS spectra and plots of [F(R)*h*v]$^{0.5}$ versus photon energy (h*v) (in the inset) of the prepared powders are given in Fig. 1(c). NMP and SMP powders showed visible light absorption (in the

Table 1 — Structural/physical properties of the prepared powders.

Powder	Anatase crystallite size (nm)	Rutile crystallite size (nm)	Rutile wt. (%)	A (Å)	C (Å)	Lattice Strain (%)	Average bulk particle size (nm)	Average pore volume (cc/g)	Average pore diameter (nm)	Specific surface area (m²/g)	Band gap (eV)
OMP	34.1	76.4	10.0	3.77	9.39	0.56	133	0.126567*	17.4*	27.3	3.05
NMP	22.6	30.4	15.9	3.77	9.35	0.48	434	0.271723**	19.9	54.5	2.93
SMP	17.8	-	0	3.78	9.31	0.78	98	0.524310**	24.8	84.5	2.93
P25	24.5	34.9	15.9	3.77	9.40	1.2	226	0.068648*	4.9*	58.1	2.94

* Data from BJH adsorption
** Data from single point
*** Crystallographic data, band gap energies and nitrogen adsorption results were "Reprinted from International Journal of Hydrogen Energy, Vol 43, Hüsnü Arda Yurtsever and Muhsin Çiftçioğlu, The effect of powder preparation method on the artificial photosynthesis activities of neodymium doped titania powders, 20162-20175, Copyright (2018), with permission from Elsevier[31].

420-520 nm wavelength range) which may originate from the possible N or S incorporation in the TiO_2 lattice or the electron transfer from surface N or S containing species to the TiO_2 conduction band[34-36]. The calculated band gap energies also indicated that NMP and SMP powders can absorb visible light. According to the results, the use of nitric acid and sulfuric acid likely caused the formation of N or S containing species and substitutional exchange of O and Ti atoms in relatively low levels for NMP and SMP powders, respectively. Room temperature PL spectra of the powders recorded upon 285 nm wavelength excitation are given in Fig. 1(d). The spectra of the powders containing N or S species (NMP and SMP, respectively) and the powders without impurities (OMP and P25) exhibit excitonic PL signals with similar shapes. The impurities did not cause new PL phenomena, however the peak intensities showed variation. Higher PL intensities may originate from the presence of higher number of surface oxygen vacancies and the presence of fine particles that provides low distances for electrons to travel freely which facilitate the formation of excitons by binding of electrons[37, 38]. Thus PL intensity may be affected by both the particle size and number of surface oxygen vacancies. PL intensity of the OMP powder has the highest value at 394 nm, compared to the other powders including commercial powder Degussa P25. Oxygen vacancies on the surface are known to contribute the surface reactivity as well as the particle size, phase composition, band gap energy and surface states of the present elements. Thus there is an optimum configuration for these properties in order to obtain high surface reactivities.

Surface area analysis results presented in Fig. 2 and Table 1, showed that powders showing similar porous structure with commercial powder P25 were prepared by the chemical precipitation method used in this study. Nitrogen adsorption-desorption isotherms of
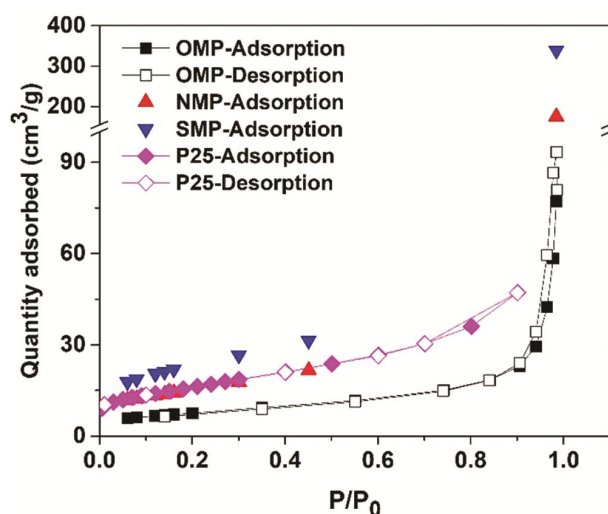
Fig. 2 — Nitrogen adsorption-desorption isotherms of OMP and P25 powders, nitrogen adsorption isotherms of NMP and SMP powders.

OMP powder (Fig. 2) presented a typical Type IV BDDT (Brunauer–Deming–Deming–Teller) isotherm with an H3 type hysteresis loop indicating that this powder is a mesoporous material[39]. The highest surface area and the highest pore volume was obtained with SMP powder which may be due to the inhibition of phase transformation caused by the presence of sulfur containing species in the nanostructure[40]. The lowest surface area was obtained with OMP powder which has the highest crystallite sizes for both anatase and rutile phases. These results along with the phase structure analysis results showed that OMP powder has the highest activity(had an enhanced nanostructure evolution behavior at 600°C) compared to the other powders.

According to the phase structure, surface area related properties and light absorption characteristics, a Degussa P25 like photocatalyst was prepared by applying chemical precipitation in nitrate
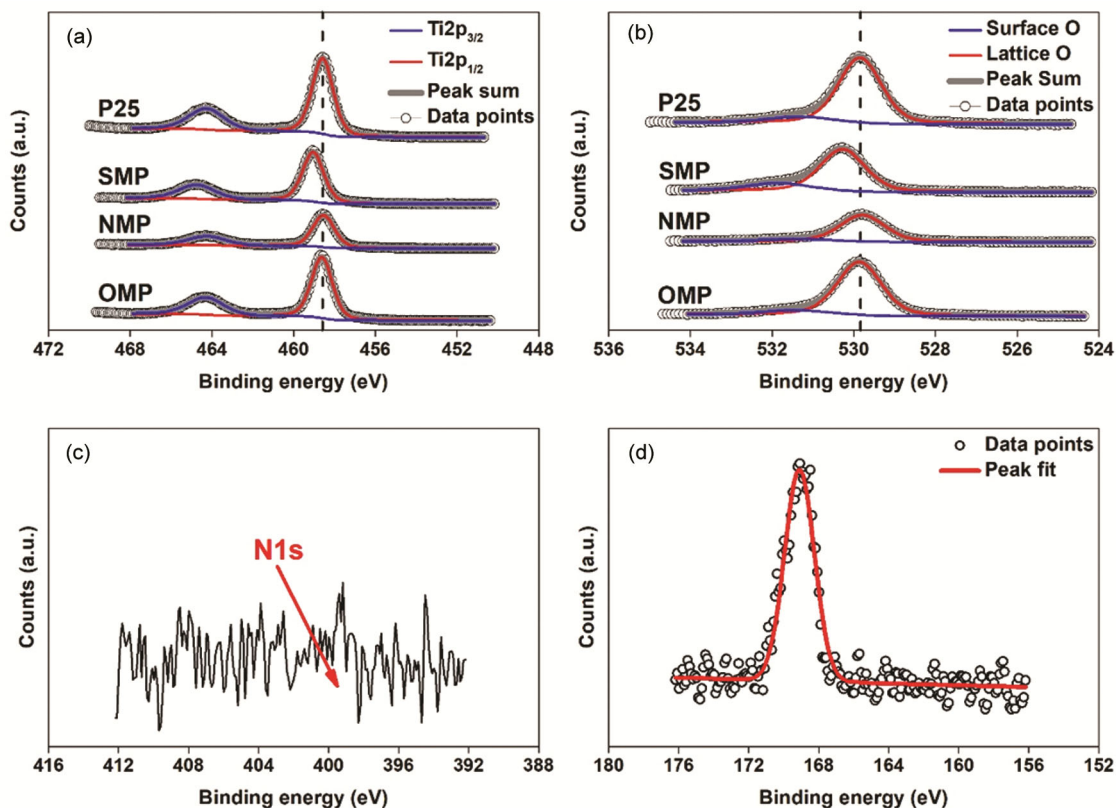
Fig. 3 — (a) Ti2p; (b) O1s XPS spectra of the prepared powders; (c) S2p XPS spectrum of SMP powder and (d) N1s XPS spectrum of NMP powder. XPS data were "Reprinted from International Journal of Hydrogen Energy, Vol 43, Hüsnü Arda Yurtsever and Muhsin Çiftçioğlu, The effect of powder preparation method on the artificial photosynthesis activities of neodymium doped titania powders, 20162-20175, Copyright (2018), with permission from Elsevier[31]

medium (NMP) and at the heat treatment temperature of 600 °C.

Ti2p, O1s spectra of the prepared powders and S2p and N1s XPS spectra of SMP and NMP powders, respectively, are given in Fig. 3 (a-d), respectively. All the peak positions were corrected according to C1s peak position shifts. The prepared powders consist of Ti^{4+} oxidation state according to the peaks at 529 and 531.5 eV which correspond to $Ti2p_{1/2}$ and $Ti2p_{3/2}$, respectively [Fig 3(a)]. Signals appearing at 529 and 531.5 eV are attributed to the lattice oxygen and surface hydroxyls, respectively [Fig 3(b)]. $Ti2p_{3/2}$ binding energies were similar for OMP, NMP and P25, but the highest for SMP which shows that Ti-S bonds which have higher binding energies were formed due to the presence of S containing species or to substitutional S doping at low levels. Signal appearing at 169 eV for SMP powder was attributed to S^{6+} originating from the presence of S containing species [Fig 3(d)]. The absence of S^{2-} signal at 163 eV may indicate that there were no partial substitution of

O atoms by S atoms or not detected due to the presence of very low levels[41]. The substitution of Ti^{4+} (0.068 nm) with S^{4+} (0.037) or S^{6+} (0.029) is more favorable than replacing O^{2-} with S^{2-}[42]. A small amount of substitution may also be the cause for the difference in the UV-Vis DRS spectrum as discussed earlier. N1s spectrum of the NMP powder [Fig 3(c)] indicated a peak with a relatively low intensity at ~400 eV which may be due to Ti-O-N bonding[43] and interstitial N doping[44]. Nitrogen may also be considered to substitute oxygen in the lattice at low levels according to the combined results of XRD, UV-Vis DRS and XPS.

Photocatalytic degradation of synthetic dyes and real textile wastewater

Various synthetic dyes were used in order to evaluate the influence of surface properties on the surface reactivity of TiO₂ powders. Surface-normalized degradation (C_S) and $\ln(C_0/C)$ versus time plots for methylene blue [Fig. 4(a & b)], methyl orange [Fig. 4(c & d)] and rhodamine B [Fig. 4(e & f)] dyes are given in Fig. 4. The highest surface
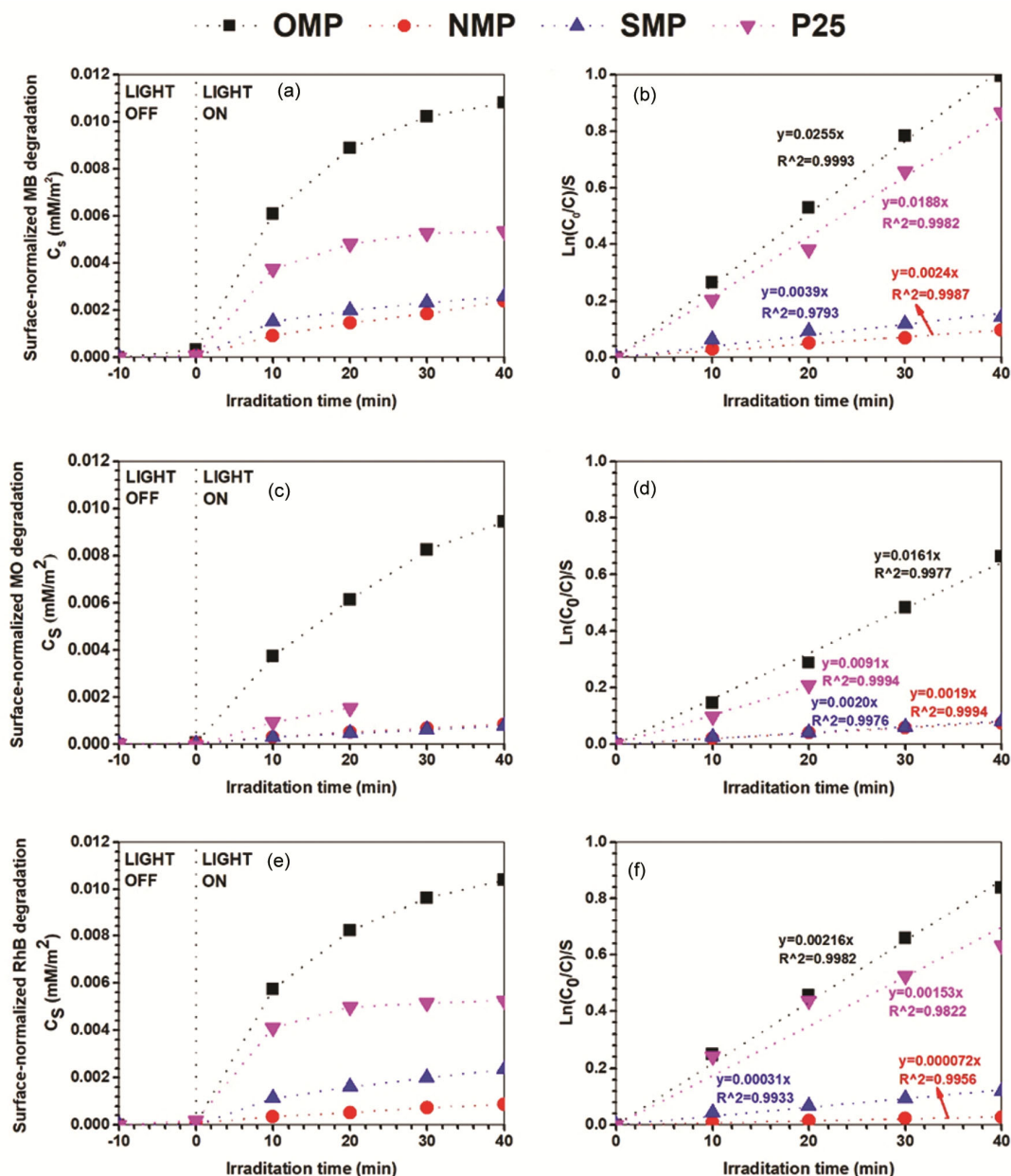
Fig. 4 — Surface-normalized degradation (C_S) and $\ln(C_0/C)$ versus time plots of the powders: (a, b) methylene blue, (c, d) methyl orange and (e, f) rhodamine B.

reactivity was obtained with OMP powder which has the highest anatase and rutile crystallite sizes with lower rutile weight percentage compared to NMP and P25. The lowest activities were obtained with NMP and SMP powders. OMP powder showed slightly better performance in the photocatalytic CO_2 reduction where as NMP powder showed significantly better performance in photocatalytic H_2 production when compared to P25 in our previous study[31]. Since

oxidation and reduction proceeds on different reaction mechanisms, the activities of the powders may be variable in oxidation (dye degradation) or reduction (artificial photosynthesis) reactions.

Normalizing the photocatalytic activities with specific surface areas give the opportunity to evaluate the influence of surface chemical and physical properties on the photocatalytic activity. The characterization results showed that NMP powder

exhibit Degussa P25 like properties with regard to crystalline phase composition, crystallite size, surface area and light absorption characteristics. These properties are vital in photocatalysis. However, the surface reactivity of NMP powder was found to be lower than that of P25 for all kinds of synthetic dyes. P25 powder is known to be almost pure whereas NMP powder contains nitrogen impurities at low level (supported by XPS and UV-Vis DRS) which may have significant effects on the surface reactivity. OMP powder may be as pure as P25 since the precipitation medium of OMP powder is completely

composed of organic solvent and precursor which may have decomposed to CO_2 at $600^{\circ}C$ leaving no impurities in the final oxide powder. There are studies which showed the positive effects of nonmetals doping on the photocatalytic activity of TiO_2[9, 10]. Our results indicated that N or S impurities have negative effects on the surface reactivity of TiO_2.

The UV-Vis absorption spectra of the original and diluted RTW solutions are given in Fig. 5(a). The spectra of the waste water samples showed that RTW has a broad absorption in visible light region and maximum absorption was at 424 nm. Total carbon (TC), total organic carbon (TOC) and inorganic carbon (IC) amounts of the RTW solutions and the UV-Vis absorbance values at 424 nm of the solutions are given in Fig. 5(b). Linear curves were obtained with dilution for all the aforementioned properties and it was found that 1/5 diluted RTW (0.2RTW concentration) has ~10 mg/L (ppm) TOC content. All the photocatalytic runs were performed with 1/5 diluted RTW as it is a standard in photocatalysis (and also 10 ppm methylene blue, methyl orange and rhodamine B dye solutions were used in this study) to use 10 ppm initial substrate concentration.

RTW removal by adsorption and photocatalysis curves, $\ln(C_0/C)$ curves and surface-normalized 1st order reaction rate constants of the powders for different dyes are given in Fig.6 (a-d), respectively. RTW adsorption and photocatalytic removal efficiencies (%) in 1 h, the final *p*H, conductivity and Pt-Co colour values of the corresponding treated waste water samples are given in Table 2.

The order of the removal %s of RTW was determined to be as SMP=P25>OMP>NMP for both adsorptive and photocatalytic removal (Table 2). Adsorption was almost stabilized after ten minutes for all the powders and 21, 9, 24 and 25% of the RTW were adsorbed at the end of 1 hour with OMP, NMP, SMP powders and P25, respectively [Fig. 6(a)]. Adsorption %s of the powders are well correlated with the powder surface area. Highest

Fig. 5 — (a) UV-Vis absorption spectra and (b) TOC/TC/IC and UV-Vis absorbance at 424 nm curves of the RTW solutions.

Table 2 — RTW removal efficiencies, final pH, conductivity and Pt-colour values of the treated RTW with the powders.

Powder	RTW removal efficiency by adsorption in 1 h	RTW removal efficiency by photocatalysis in 1 h	Final *p*H	Final conductivity (mS/cm)	Final colour (Pt-Co)
	(%)	(%)			
OMP	21	96	7.6	2.81	20
NMP	9	78	7.7	2.51	55
SMP	24	99	7.8	2.46	10
P25	25	99	7.8	2.45	21
Photolysis	-	1	-	-	-
1/5 RTW*			8.6	2.48	231
* Initial *p*H, conductivity and Pt-colour values for 1/5 RTW.					
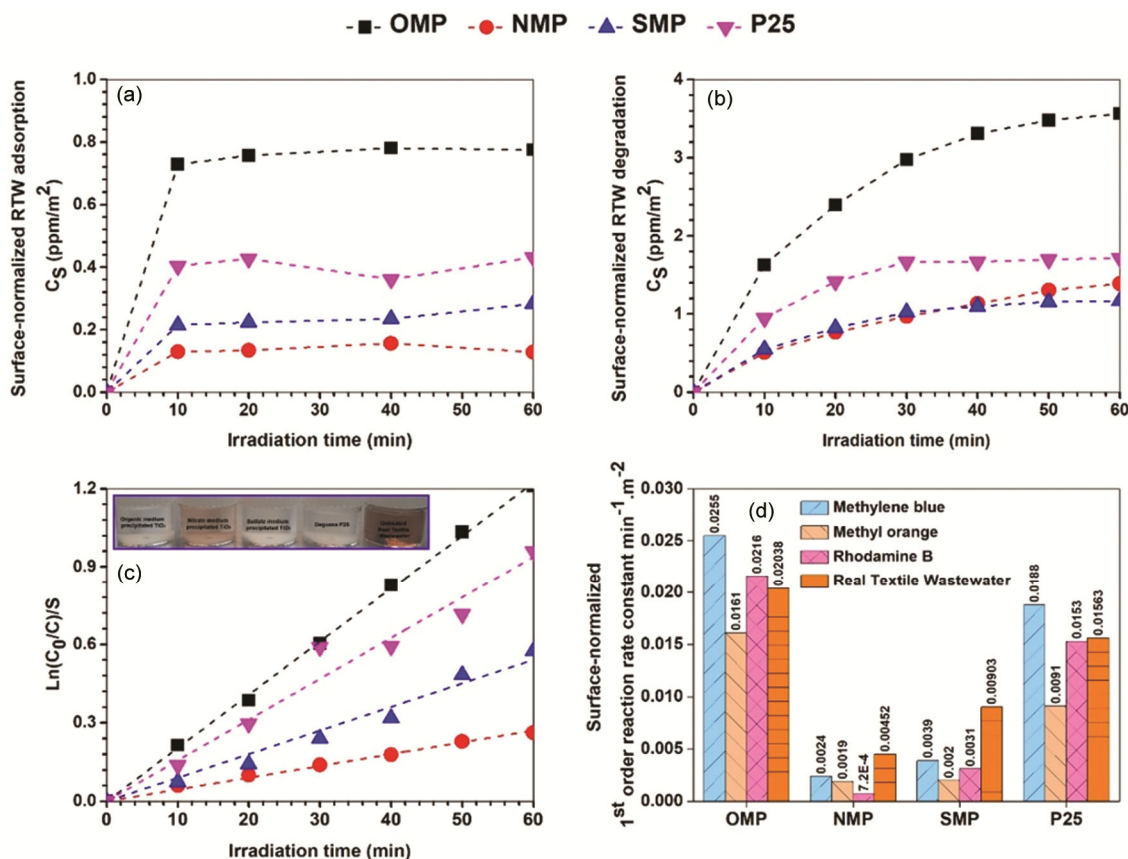
Fig. 6 — (a, b) RTW removal by adsorption and photocatalysis curves, (c) $\ln(C_0/C)/S$ curves and in the inset: photographs of the treated RTW samples at the end of 1 h and (d) surface-normalized 1st order reaction rate constants of the powders.

adsorption levels were obtained with the SMP powder and P25 which exhibit the highest surface areas.

RTW was nearly 100% degraded by photocatalysis in 1 hour with OMP, SMP and P25 powders (Table 2).The magnitude of the surface-normalized rate constant changes in the following order:OMP> P25>SMP>NMP [Fig. 6(b) and 6(d)]. NMP and SMP have lower bandgap energies compared to OMP which shows that they can utilize a higher number of photons compared to OMP powder; however they have the lowest surface-normalized rate constants. It was observed that the surface reactivity of the SMP powder was relatively lower than the other powders which may be due to its smaller average crystallite size as reported elsewhere[45,46]. Low anatase-rutile ratio can also decrease the activity since anatase has more photocatalytic activity than rutile[47,48]. The presence of rutile however can increase the absorption of light since it has a smaller band gap energy compared to anatase. It was shown that surface reactivity of TiO_2 can be increased with the applied heat treatment temperature which increases the

crystallite size and favors rutile phase formation[49]. However, it was also shown that increased amounts of rutile phase in the nanostructure may decrease the surface reactivity. Thus it is important to obtain the optimum level of phase composition. OMP powder may have more suitable anatase and rutile crystallite sizes (highest) and rutile wt. % (lowest) compared to NMP, SMP and P25. Previously, it was stated that PL analyses indicated the presence of more oxygen deficiencies in OMP powder. This may improve the photo generated charge carrier separation capability of OMP and make it photocatalytically more active than the other powders[50]. S and N species on the grain boundaries (SMP and NMP powders, respectively) increased both the light absorption and the surface areaofTiO_2 which are very important parameters in photocatalysis. The surface reactivities of the SMP and NMP powders were determined to be lower compared to OMP powder which has higher bandgap energy and lower surface area. This may indicate that the rate of charge carrier transport facilitated by suitable crystallite size and the presence of anatase-
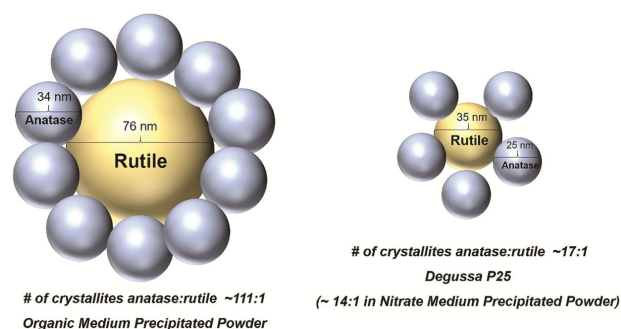
Fig. 7 — Schematic representation of the proposed crystalline phase structure of the synthesized powders and Degussa P25.

Fig. 8 — Schematic representation of the main conclusion of this study.

rutile heterojunctions have a very important role in photocatalytic processes. It is therefore likely that there is an optimum composition of the crystalline phase structure, physicochemical and electronic properties for achieving the maximum surface reactivity.

Conductivity, pH and Pt-Co colour values of treated wastewater (given in Table 2) are known to be important parameters in developing new wastewater treatment technologies since they demonstrate the level of the efficiency of the treatment process and the reusability of the wastewater. Final pH and conductivity values were found to be nearly same for all the powders. Final Pt-Co colour values were found to be in the following order NMP>OMP=P25>SMP. According to these findings, this study suggests that OMP powder which has lower specific surface area compared to that of other powders, may conduct the photocatalytic removal of synthetic dyes and RTW with almost the same efficiency as the powders with higher surface areas by the help of its high surface reactivity. This study revealed that OMP powder based coatings can be good candidates to be used in wastewater removal processes. The crystalline phase structure (the highest anatase and rutile crystallite sizes and low rutile weight percentage) may be the main reason that facilitates the charge carrier separation and increase the rate per surface area in the degradation of synthetic dyes and RTW.

A representative phase structure was proposed as shown in Fig. 7. The volumes of the anatase and rutile phases were drawn according to the calculated crystallite sizes presented in Table 1. The number of anatase and rutile crystallites were calculated roughly by using the densities of anatase (3.85 g/cm^3) and rutile (4.23 g/cm^3), the mass percentages given in Table 1 and assuming the crystallites are in spherical shapes. The exact number of crystallites could not be presented in the figure since the differences are very
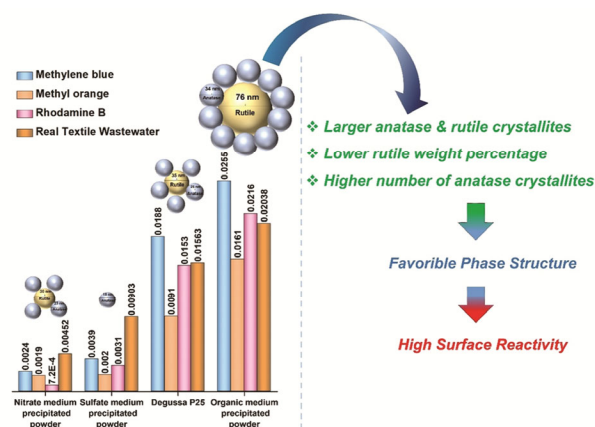
high (e.g. 111:1). According to the representative figure and the results of this study, a nanophase structure with large anatase and rutile crystallites where the number of anatase crystallites are much more than rutile crystallites may have high photocatalytic performance in the degradation of synthetic dyes and real textile wastewater even the structure possess high band gap energy and low surface area. Main conclusion of this study is schematically shown in Fig. 8.

Conclusion

In this study TiO$_2$ photocatalyst powders are precipitated in three different media containing N, S or organic species. The photocatalytic degradation activities of the prepared powders in the treatment of synthetic dyes and a real textile wastewater are evaluated with regard to their nanophase structure, crystallite size, surface area, light absorption and electronic properties. Using excess amounts of nitric acid and sulfuric acid in the powder preparation media induced N and S doping in the TiO$_2$ lattice, respectively. The use of sulfuric acid for the dissolution of TiO$_2$ precipitate formed by hydrolyzing TTIP led to the presence of significant amounts of residual S species on the grain boundaries along with possible substitutional S accommodation in the Ti^{4+} sites. Photocatalytic dye degradation experiments showed that photocatalytic activity strictly depends on the crystalline phase structure of the photocatalytic material. Nitrate and sulfate media precipitated powders showed lower surface reactivities even though they have lower band gap energies compared to organic medium precipitated powder. The organic medium precipitated powder exhibit the highest surface-normalized 1st order reaction

rate constants for photocatalytic degradation of various dyes. This powder show higher surface reactivities between 2 to 30 folds of the powders precipitated in N or S containing media. The surface reactivity of organic medium precipitated powder is found to be 36, 77, 41 and 30 % higher than that of the commercial powder Degussa P25 in methylene blue, methyl orange, rhodamine B and real textile wastewater degradation, respectively. The reason of the high surface reactivity of organic medium precipitated powder may be the presence of larger anatase and rutile crystallites (which is more favourable compared to low crystallite sizes cited in the literature) and the presence of a lower amount of rutile which facilitates the formation of functional anatase-rutile heterojunctions and provides a higher surface area for anatase phase which is photocatalytically more active than the rutile phase.

Acknowledgements

References

1 Factorovich M, Guz L & Candal R, *Adv Phys Chem*, 2011 (2011) 821204.
2 Zaleska A, *Rec Pat Eng*, 2 (2008) 157.
3 Pozan G S & Kambur A, *Chemosphere*, 105 (2014) 152.
4 Dugandžić I, Jovanović D, Mančić L, Zheng N, Ahrenkiel S, Milošević O, Šaponjić Z & Nedeljković J, *J Nanopart Res*, 14 (2012) 1.
5 Akpan U G & Hameed B H, *J Hazard Mater*, 170 (2009) 520.
6 Watson S S, Beydoun D, Scott J A & Amal R, *Chem Eng J*, 95 (2003) 213.
7 Xiao J, Xie Y & Cao H, *Chemosphere*, 121 (2015) 1.
8 Matos J, Ocares-Riquelme J, Poon P S, Montaña R, García X, Campos K, Hernández-Garrido J C & Titirici M M, *J Colloid Interface Sci*, 547 (2019) 14.
9 Zhou F, Song H, Wang H, Komarneni S & Yan C, *Appl Clay Sci*, 166 (2018) 9.
10 Yan J, Zhao J, Hao L, Hu Y, Liu T, Guan S, Zhao Q, Zhu Z & Lu Y, *Mater Res Bull*, 120 (2019) 1.
11 Yi C, Liao Q, Deng W, Huang Y, Mao J, Zhang B & Wu G, *Sci Total Environ*, 684 (2019) 527.
12 Wahyuni E T, Mahira N S, Lestari N D & Natsir T A, *Indian J Chem Technol*, 29 (2022) 519.
13 Khan M A M, Nain P, Ahmed J, Ahamed M & Kumar S, *Opt Mater*, 133 (2022) 112983.
14 Mishra S, Chakinala N, Chakinala A G & Surolia P K, *Catal Commun*, 171 (2022) 106518.
15 Anisha R & Kirupa V E K, *Indian J Chem Technol*, 29 (2022) 547.
16 Umadevi P, Ramya Devi K T, Sridevi D V, Perumal S & Ramesh V, *Mater Sci Eng B*, 286 (2022) 116018.
17 Xing M, Zhang J & Chen F, *Appl Catal B*, 89 (2009) 563.
18 Xu P, Xu T, Lu J, Gao S, Hosmane N S, Huang B, Dai Y & Wang Y, *Energy Environ Sci*, 3 (2010) 1128.
19 Bansal P & Sud D, *Desalination*, 267 (2011) 244.
20 Chun H & Yizhong W, *Chemosphere*, 39 (1999) 2107.
21 Gümüş D & Akbal F, *Water Air Soil Pollut*, 216 (2011) 117.
22 Gomes de Moraes S, Sanches Freire R & Durán N, *Chemosphere*, 40 (2000) 369.
23 Pekakis P A, Xekoukoulotakis N P & Mantzavinos D, *Water Res*, 40 (2006) 1276.
24 Chen C Y, Yen S H & Chung Y C, *Chemosphere*, 117 (2014) 494.
25 Giwa A, Nkeonye P O, Bello K A & Kolawole K A, *J Environ Prot*, 3 (2012) 1063.
26 Hachem C, Bocquillon F, Zahraa O & Bouchy M, *Dyes Pigm*, 49 (2001) 117.
27 Mahmoodi N M & Arami M, *J Photochem Photobiol B: Biol*, 94 (2009) 20.
28 Mahvi A H, Ghanbarian M, Nasseri S & Khairi A, *Desalination*, 239 (2009) 309.
29 Wachs I E, Phivilay S P & Roberts C A, *ACS Catal*, 3 (2013) 2606.
30 Braslavsky S E, Braun A M, Cassano A E, Emeline A V, Litter M I, Palmisano L, Parmon V N & Serpone N, *Pure Appl Chem*, 83 (2011) 931.
31 Yurtsever H A & Çiftçioğlu M, *Int J Hydrog Energy*, 43 (2018) 20162.
32 Vajda K, Saszet K, Kedves E Z, Kása Z, Danciu V, Baia L, Magyari K, Hernádi K, Kovács G & Pap Z, *Ceram Int*, 42 (2016) 3077.
33 Shah A H & Rather M A, *Mater Today: Proc*, 44 (2021) 482.
34 Di Valentin C, Finazzi E, Pacchioni G, Selloni A, Livraghi S, Paganini M C & Giamello E, *Chem Phys*, 339 (2007) 44.
35 Zhang M, Wu J, Lu D & Yang J, *Int J Photoenergy*, 2013 (2013) 1.
36 Nishikiori H, Hayashibe M & Fujii T, *Catalysts*, 3 (2013) 363.
37 Xiao Q, Si Z, Yu Z & Qiu G, *Mater Sci Eng B*, 137 (2007) 189.
38 Nithyaa N & Victor Jaya N, *Appl Phys A*, 127 (2021) 1.
39 Wang Y, Zou Y, Shang Q, Tan X, Yu T, Huang X, Shi W, Xie Y, Yan G & Wang X, *Trans Tianjin Univ*, 24 (2017) 326.
40 Sun B, Zhou G, Shao C, Jiang B, Pang J & Zhang Y, *Powder Technol*, 256 (2014) 118.
41 Yan G, Zhang M, Hou J & Yang J, *Mater Chem Phys*, 129 (2011) 553.
42 Yu J C, Ho W, Yu J, Yip H, Wong P K & Zhao J, *Environ Sci Technol*, 39 (2005) 1175.
43 Zhang K, Wang X, He T, Guo X & Feng Y, *Powder Technol*, 253 (2014) 608.
44 Peng F, Cai L, Yu H, Wang H & Yang J, J, *Solid State Chem*, 181 (2008) 130.
45 Sayılkan F, Asiltürk M, Şener Ş & Erdemoğlu S, *Turk J Chem*, 31 (2007) 211.
46 Hwang K J, Lee J W, Shim W G, Jang H D, Lee S I & Yoo S J, *Adv Powder Technol*, 23 (2012) 414.
47 Luttrell T, Halpegamage S, Tao J, Kramer A, Sutter E & Batzill M, *Sci Rep*, 4 (2014) 1.
48 Zhang J, Zhou P, Liu J & Yu J, *Phys Chem Chem Phys J*, 16 (2014) 20382.
49 Chen W T, Chan A, Jovic V, Sun-Waterhouse D, Murai K, Idriss H & Waterhouse G I N, *Top Catal*, 58 (2015) 85.
50 Tan H, Zhao Z, Zhu W-b, Coker E N, Li B, Zheng M, Yu W, Fan H & Sun Z, *ACS Appl Mater Interf*, 6 (2014) 19184.